Phase dependence of Kerr-based parametric amplification

Nathan G. Drouillard and T. J. Hammond*
Department of Physics, University of Windsor, Windsor, Ontario, Canada N9B 3P4

(Received 1 May 2024; accepted 6 August 2024; published 20 August 2024)

Kerr instability amplification can amplify over an octave of spectrum, a broad bandwidth supporting few-cycle pulses. However, dispersion management in this regime is crucial, and we explore the parameters required to maintain the ultrashort pulse undergoing amplification. At low pump intensities, we experimentally observe an interference between the strongly chirped supercontinuum seed and weakly amplified pulse, reproduced in our model by manipulating the seed dispersion. Extending our model to cases of high gain, our simulation predicts the dispersion is near zero, and the phase can be compensated preamplification to generate near-transform-limited amplified few-cycle pulses. We discuss chirping the seed pulse to avoid saturation, a route for generating sub-mJ few-cycle pulses in a single stage from Kerr instability chirped-pulse amplification.

DOI: 10.1103/PhysRevA.110.023517

I. INTRODUCTION

Recently, theory and experiments of Kerr instability amplification (KIA) demonstrated the amplification of supercontinuum spectra spanning nearly an octave in bandwidth in a single beam [1–3]. Such broadband spectra support few-cycle pulses, where the peak-field strength depends on both the dispersion and the carrier envelope phase (CEP) [4–6]. Broadband amplified spectra drive intense ultrafast experiments such as high harmonic generation, strong-field physics, and attosecond (1 as $= 10^{-18}$ s) science [7–9]. Femtosecond (1 fs $= 10^{-15}$ s) amplifiers must amplify the broad spectrum without introducing spurious temporal and spatial phase effects that would compromise the pulse coherence.

Chirped pulse amplification (CPA) enables large gain over a broad bandwidth by temporally dispersing the seed pulse, stretching it to decrease the peak intensity and avoid multiphoton absorption and optical damage in the gain medium [10,11]. The amplified pulse is then subsequently recompressed to undo the initial dispersion, leading to intense fs pulses. However, the limited gain medium bandwidth leads to gain narrowing with each pass in the amplifier [12–14].

Optical parametric amplifiers (OPAs) can side-step this gain narrowing by several means. A noncollinear geometry (NOPA) can substantially increase the gain bandwidth, leading to amplified spectra that support few-cycle pulses [15]. Multiple amplification stages can be combined with other nonlinear processes to create intense few-cycle pulses with central wavelengths from the visible to the midinfrared [16–18]. Fourier-domain amplification (FOPA) tailors the gain of each spectral component, allowing for spectral shaping and tuning [19,20]. However, these OPAs require crystals with large second-order nonlinearity $\chi^{(2)}$, limiting the choice of available gain media.

Conversely, KIA relies on the third-order nonlinearity $\chi^{(3)}$, which is present in all materials, and can amplify supercontinuum spectra that support few-cycle pulses in a single step without additional pulse shaping. Furthermore, the parametric amplification process automatically allows for excellent pulse contrast without requiring pulse picking, making it a suitable seed for petaWatt scale few-cycle sources [21]. The theory of KIA is derived elsewhere [22], and our previous work shows that KIA theory can be reproduced by extending the definition of four-wave mixing (FWM) [3] to directly amplify a supercontinuum spectrum in a single beam [2].

As with any nonlinear process, FWM requires conservation of energy ($2\omega_p = \omega_s + \omega_i$, where $\omega_{p,s,i}$ are the pump, signal, and idler frequencies, respectively) and momentum ($2\mathbf{k}_p = \mathbf{k}_s + \mathbf{k}_i$, where $\mathbf{k}_{p,s,i}$ are the respective wave vectors) [23]. We modify the FWM phase matching condition by accounting for the material nonlinearity,

$$k_p^2 = \frac{\omega_p^2}{c^2}\left(n_p^2 + n_2 I_p\right), \tag{1}$$

where $n_p = n(\omega_p)$ is the index of refraction at the pump frequency, n_2 is the nonlinear Kerr coefficient of the material related to $\chi^{(3)}$, and I_p is the peak pump intensity. This new definition modifies the noncollinear phase matching condition for FWM, leading to an internal output angle of the signal given by

$$\cos\theta_s = \frac{4\left(n_p^2 - n_2 I_p\right)\omega_p^2 + n_s^2\omega_s^2 - n_i^2\omega_i^2}{4n_s\omega_s\omega_p\sqrt{n_p^2 - n_2 I_p}}. \tag{2}$$

Without an intensity-dependent index, the FWM phase-matching condition predicts collinear phase matching at the pump wavelength [24], a significant difference between FWM and KIA. Using our extended definition of FWM, we effectively model KIA, where the gain g of the seed is given by

$$g \approx \frac{\omega_p}{c}\frac{n_2}{n_p} I_p\left[2 - \cosh\left(\frac{\omega - \omega_p}{\omega_p}\right)\right]. \tag{3}$$

*Contact author: tj.hammond@uwindsor.ca

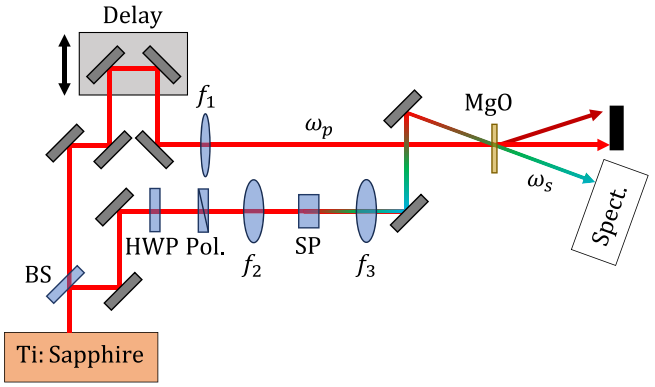

FIG. 1. Setup for KIA in 0.5 mm MgO. A BS first splits the output of a Ti:sapphire laser to create the pump (ω_p) and the seed (ω_s). The pump overlaps with the supercontinuum seed at an external interaction angle of 5.3° in 0.5 mm MgO. The resulting amplified pulse is measured with a spectrometer (spect.). See text for details.

However, the first ∼100 μm of propagation does not amplify the seed, but rather creates the idler. Therefore, the signal and idler intensities, in the undepleted pump approximation, are [25]

$$I_s(z) \approx I_s(0)\cosh^2\left(\frac{g}{2}z\right), \tag{4}$$

$$I_i(z) \approx \frac{\omega_s}{\omega_i} I_s(0)\sinh^2\left(\frac{g}{2}z\right). \tag{5}$$

When the amplification $I_s(z)/I_s(0)$ is found, the gain is then calculated by isolating for g.

We propose that since KIA has a larger gain and bandwidth than the first stage of multistage $\chi^{(2)}$ parametric amplifiers [18,26,27], it could be used to replace this first stage for few-cycle pulses. However, several phase effects must be studied to ensure that the phase is maintained without introducing significant field distortion.

In this work, we present an experimental result showing an interference between the seed and amplified pulses. We create a numerical model that agrees with our experimental findings, and use this model to simulate the amplification by Kerr instability to study the effects of amplification on the phase. We investigate the dispersion in the amplification process and how controlling the seed phase allows for amplified few-cycle pulses near the transform limit. We also discuss the effect of the seed and pump CEP on the amplified pulse, as well as pump intensity jitter. Although saturation distorts the amplified pulse, we can avoid this effect by prechirping the pulse to decrease the seed peak intensity, enabling Kerr instability chirped-pulse amplification (KICPA).

II. AMPLIFIED PULSE PHASE

The setup for the experiment is shown in Fig. 1. We use a Ti:sapphire laser that outputs 110 fs pulses at 1 kHz, centered at 785 nm. A beamsplitter (BS) splits the beam into two paths to create the seed and pump. A half-wave plate (HWP) and polarizer (Pol.) control the seed energy (1 μJ) into the 5-mm sapphire plate (SP). The resulting seed supercontinuum spectrum spans from 450 to 1000 nm at 50 dB (see Ref. [2] for further details). A BK7 lens collimates ($f_3 = 25$ mm) and refocuses the supercontinuum onto the 0.5 mm MgO. The pump arm sits on a delay stage to control the timing between pump and seed, and is focused using a $f_1 = 300$ mm lens ($w_0 \approx 70$ μm) onto the 0.5 mm MgO. The pump pulses have an average pulse energy of 127 μJ, resulting in the estimated peak intensity of $I_p = 8 \pm 1 \times 10^{16}\,\mathrm{W/m^2}$. The pump and seed interact at an external angle of 5.3 ± 0.2° in the MgO crystal, resulting in amplification. The spectrum of the amplified seed supercontinuum (ω_s) is measured using an Ocean Optics Flame-S spectrometer. The residual pump and idler are also shown, but not measured.

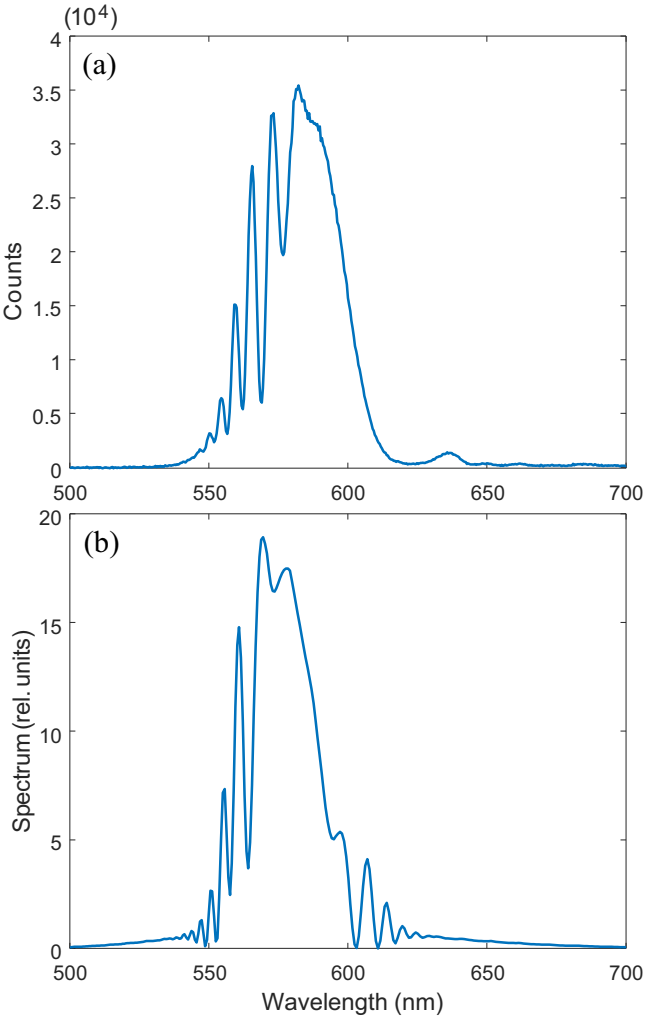

FIG. 2. (a) Experimental amplified spectrum centered at 580 nm, showing interference fringes on the blue side of the spectrum when pumped at low power. (b) Numerical result for the amplified spectrum of a 5-fs pulse centered at 580 nm.

At low gain, we observe inteferences fringes in the spectrum of the amplified pulse. Figure 2(a) shows our experimental result for amplifying a seed pulse centered at 580 nm with the experimental conditions stated above. In this low-intensity, low-gain regime, we observe interference fringes on the blue side of the amplified spectrum, suggesting an interference between the seed and amplified pulses. To understand this interference, we perform simulations to investigate the phase of the amplified pulse.

Having performed experiments, we develop a numerical model to further understand our experimental result, and the remainder of this work will report on pulse propagation simulations. Our simulations are performed in two dimensions to account for the transverse phase-matching criterion. We solve the forward Maxwell equation (FME) in two dimensions [28,29] by fourth-order Runge-Kutta (RK4), fast Fourier transforming from position to momentum space for wavefront propagation [2,3]. FME is written in the spatial-frequency domain as

$$\frac{\partial}{\partial z}E(\vec{r},\omega) = i\frac{c}{2n(\omega)\omega}\nabla_T^2 E(\vec{r},\omega) + i\frac{\omega}{c}[n(\omega)-n_g]E(\vec{r},\omega) + i\frac{\mu_0\omega c}{2n(\omega)}P_{NL}(\vec{r},\omega), \tag{6}$$

where $\nabla_\perp^2 = \frac{\partial^2}{\partial x^2}$ is the transverse coordinate, $n(\omega)$ is the frequency-dependent index of refraction, and n_g is the group index evaluated at the seed central wavelength. We consider the instantaneous nonlinear polarizability, $P_{NL} = D\epsilon_0\chi^{(3)}|E|^2E(x,t)$, and the material polarization. We use the prefactor $D = 3/8$, which is consistent with Ref. [25]. We use a nonlinear Kerr coefficient $n_2 = 3\chi^{(3)}/[4\epsilon_0 c n_p^2] = 4\times 10^{-20}$ m^2/W. We previously found consistent agreement between KIA theory and our simulations for amplitude and angle dependence [3]. We now use these simulations to investigate the phase dependence of KIA.

Figure 2(b) shows the numerical result of pumping at 9×10^{16} W/m^2, with a 100 fs, 800-nm pump pulse. The seed pulse is centered at 580 nm with a pulse duration of 5 fs and the interaction angle between pump and seed is 5.3° in 0.5 mm MgO. We apply a group-delay dispersion (GDD) of 1150 fs^2/mm + 450 fs^2/mm, and a third-order dispersion (TOD) of 490 fs^3/mm to the seed pulse prior to amplification, which models the dispersion of the supercontinuum seed and that imparted by the two lenses in our experimental setup [2]. Under these conditions, we reproduce the interference fringes, suggesting that our model accurately portrays our experimental findings.

We use this agreement to understand the phase dependence of the amplification process by discussing the amplification in the time domain. Because the supercontinuum seed is strongly chirped and much longer than the pump, changing the relative seed-pump delay allows us to control the seed spectral components overlapping with the pump, where the overlap selects the portion of the spectrum to be amplified. However, because the Kerr-based amplification strongly depends on the pump intensity, the amplified pulse duration can be shortened to approximately $1/\sqrt{3}$ of the pump duration [30]. This effect is similar to the pulse shortening experienced during cross-polarized wave generation, also a $\chi^{(3)}$ process [31,32]. This pulse shortening leads to a different phase from the initial seed; in the low-amplification case we observe interference between the unamplified chirped seed and the shortened amplified pulse, leading to the interference fringes. We find that the interference fringe position depends on the pump-seed delay and is indepenent of the absolute phase of the seed and pump.

Having established a model that accurately explains our experimental results at low intensity, we extend our work to the high-intensity regime. When pumped at high intensity, MgO has shown to have a nearly constant angle that maximizes the amplification over an octave of bandwidth [2,3]. Our model does not take into account plasma effects, although we operate in the intensity regime where a plasma may be created. We note that the magnitude of change in the index of refraction that would be induced by a plasma is comparable to that of the Kerr nonlinearity at this intensity, but with opposite signs [2,33]. A plasma-induced index change may improve pump pulse propagation which would otherwise be limited by self-focussing, but it may also reduce amplification efficiency. The role of plasma creation under these conditions requires further investigation.

III. AMPLIFIED PULSE DISPERSION

For the remainder of this work, we simulate the amplification of few-cycle pulses at a constant angle of 4.5° (external angle) in 0.5 mm MgO when pumped at 1064 nm with peak intensity of 1.5×10^{17} W/m^2, unless otherwise specified. The angle optimizing the supercontinuum amplification, according to Eq. (2) is pump-wavelength dependent and is less than the 785-nm pump case discussed previously. Having used our model to reproduce our experimental results, we choose a longer wavelength for the following simulations due to the prevalence of 1040- to 1070-nm pumps in new OPCPA systems [34], and at 1064 nm the amplified pulse has a broader bandwidth.

In Fig. 3, we simulate amplifying ultrashort seed pulses centered at 970 nm to understand the effect of seed bandwidth on the amplified spectrum and phase. For the amplified spectra in Fig. 3(a), we find that there is negligible change for spectra supporting pulses as short as 10 fs full width at half maximum (FWHM) in duration by comparing the seed (double line) to amplified (single line) spectra. Gain narrowing for few-cycle pulses increases the pulse duration from 5 fs to 6.2 fs in the transform limit (TL). In all three cases, the relative amplification factor is 4400× at 970 nm, or a gain of $g = 19.6$/mm, calculated by solving for g in Eq. (4).

The initial ∼112 μm does not lead to the seed (signal) amplification, but rather idler creation [3]. Once the idler reaches the amplitude of the seed, the GDD becomes much less than that of the material. In Fig. 3(b), we show that the GDD near the pump wavelength is 10.1 fs^2, significantly less than given by the material, 26.4 fs^2 (dot dashed black). While KIA predicts zero GDD at the pump wavelength [22], higher-order terms still contribute. Near the pump wavelength, TOD estimates the dispersion; away from the amplified peak, the dispersion also depends on the spectral bandwidth and shape, as shown by the amplified bandwidths of 20 (dotted yellow), ten (dashed orange), and five (solid blue) fs pulses.

Because the dispersion is smooth over the majority of the amplified pulse bandwidth, we can compensate for it to amplify compressed pulses. Although laser amplifiers compensate for the dispersion postamplification, such as with CPA, we demonstrate here in our simulations that it is possible to compensate preamplification, maximizing the usable peak power. As shown in Fig. 4, the transform limited (TL) amplified pulse increases in duration to 6.2 fs (from a 5-fs seed). Including the amplification dispersion, the

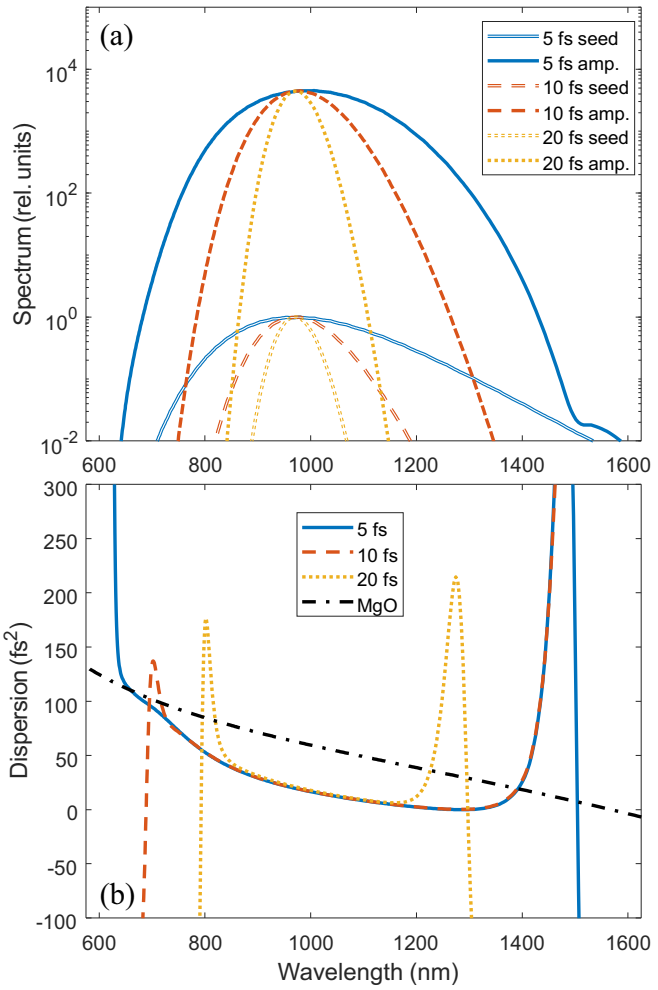

FIG. 3. Amplification and GDD of 5, 10, and 20 fs pulses centered at 970-nm from 1064-nm pump; noncollinear angle is 4.5° external angle. (a) The pulse durations are 6.2 fs (8.9 fs), 10.4 fs (11.3 fs), and 20.0 fs (20.2 fs) for the five (solid blue), ten (dashed orange), and 20 fs (dotted yellow) amplified pulse cases for transform limit (including GDD). (b) The dispersion of the amplified pulses follows a similar spectral dependence over the amplified portion of the spectrum, and is lower than the material dispersion imparted by 0.5 mm of MgO (dot dashed black) over a substantial portion of the bandwidth.

pulse duration becomes 8.9 fs. We can compensate for the amplified pulse phase by shaping the seed, fitting its phase to a sixth-order polynomial (accounting for GDD and higher orders) [35–37]. This amplified pulse duration is 6.5 fs, or two-cycle at 970-nm central wavelength.

IV. CARRIER ENVELOPE PHASE

In spite of the significant dispersion imparted by the stretching and compression steps of chirped-pulse amplification in laser amplifiers, the carrier envelope phase (CEP) of the seed oscillator is maintained. Although the amplification process itself can increase in the CEP jitter to 100 mrad [38–40], drifts can be compensated by stabilizing the oscillator CEP, pump intensity control, and other feedback (and feedforward) mechanisms [41–43].

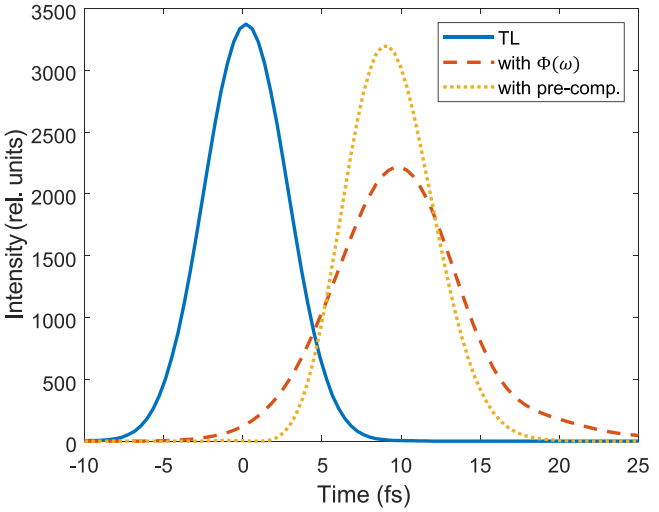

FIG. 4. A 5-fs 970-nm seed pulse amplified to transform limited duration (solid blue) 6.2 fs, accounting for phase (dashed orange) becomes 8.9 fs. By precompensating for the GDD incurred by the amplification process (dotted yellow), the pulse duration is 6.5 fs. A sixth-order polynomial fits the dispersion of the amplified pulse, and its negative is applied to the seed pulse to precompensate for the dispersion.

In our simulations, we find a similar effect in that the CEP of the oscillator was directly related to the CEP of the amplified pulse. As shown in Fig. 5, we follow the amplified field (relative to the seed magnitude) in the time domain as a function of the initial seed CEP. The carrier frequency has a period of 3.2 fs; the field peak changes by 3.2 fs while maintaining the same field envelope as the seed changes by 2π, indicating that the two are directly correlated. We note that in a similar simulation performed by changing the pump CEP, the amplified field phase is independent. Because the ideal pump would be significantly longer in duration than the seed,

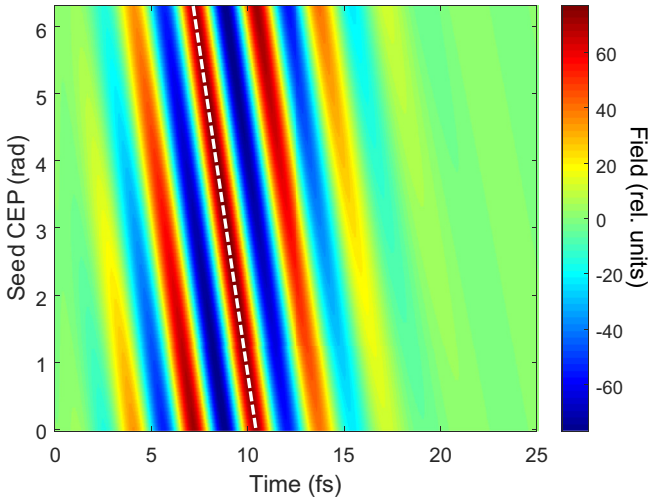

FIG. 5. Dependence of the amplified field phase on seed CEP. The linear relationship between the peak amplified field and the seed CEP (white dashed line to guide the eye) shows that the amplification process maintains the phase.

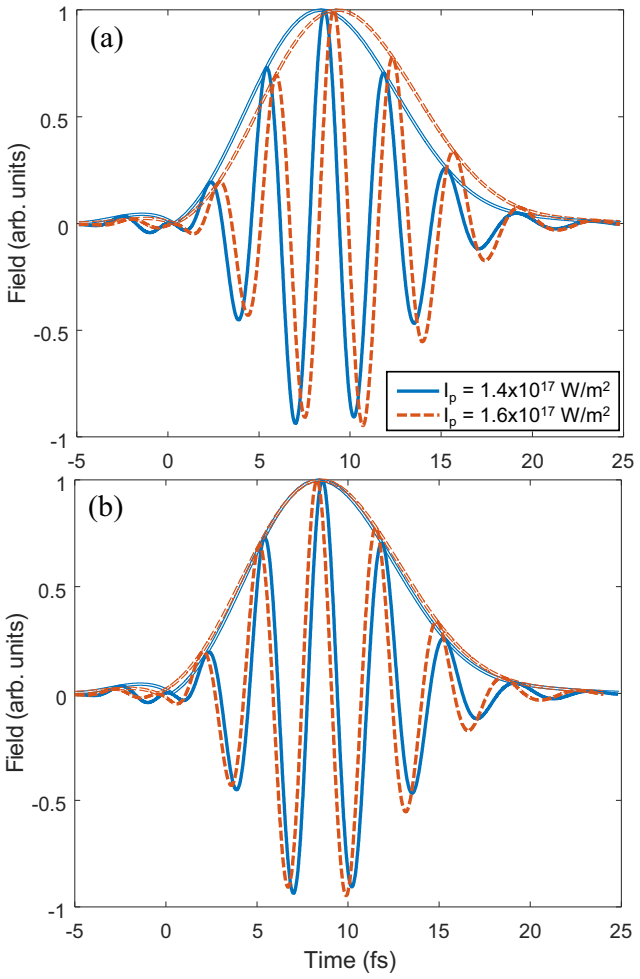

FIG. 6. Effect of pump intensity on amplified pulse phase; the seed dispersion is precompensated. (a) There is a 780 as delay in the envelope as the pump intensity increases from 1.4 (solid blue) to $1.6 \times 10^{17}\,\mathrm{W/m^2}$ (dashed orange) or 55 as/% pump intensity change. (b) After correcting the group delay to align the envelopes (double line), we also measure a CEP shift of 0.54 rad over this intensity range or 38 mrad/% pump intensity change.

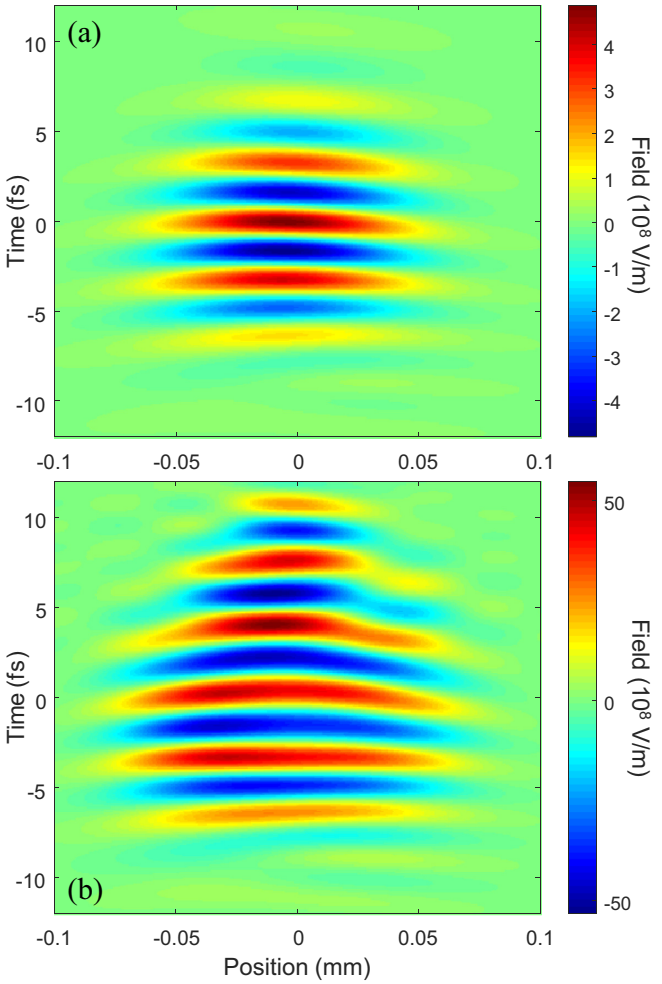

FIG. 7. Saturation effects on the spatiotemporal field evolution. (a) Relative seed intensity $I_s/I_p = 10^{-6}$ leads to a compressed amplified pulse without spatial chirp. (b) When $I_s/I_p = 6.25 \times 10^{-4}$, as the amplified pulse intensity reaches >1% of the pump (amplification factor $\approx 10^4$), the amplification is saturated and the field becomes distorted leading to walkoff and increased duration.

the pump CEP independence benefits the simplicity of the amplification scheme because of the difficulty in stabilizing narrow bandwidth pulses.

The amplified pulse CEP depends on the pump intensity, however. As the pump intensity increases from 1.4 to $1.6 \times 10^{17}\,\mathrm{W/m^2}$, there is an increased group delay of 780 as, as shown in Fig. 6(a). This group delay agrees with the expected delay due to the nonlinear index

$$T_d = \frac{L}{c}\frac{n_2}{n(\omega_p)}\Delta I_p, \tag{7}$$

where ΔI_p is the pump intensity jitter. Compared to the pump intensity of $1.5 \times 10^{17}\,\mathrm{W/m^2}$, this corresponds to a 55 as/% pump intensity change. This pump intensity to delay jitter could lead to difficulty in optical heterodyne detection experiments [44].

After compensating for this jitter, there is also a CEP change of 0.54 rad over this intensity range, or 38 mrad/% pump intensity change. For CEP-dependent experiments, KIA will benefit from pump lasers with well-controlled pulse power. The CEP jitter stems from the intensity-dependent phase matching criterion. Because the phase-matching angle depends on the pump intensity, the emerging field also has a slight angle dependence, resulting in a shift in the CEP. Although we find this CEP change to be consistent over these parameters, we also find that the CEP change depends on the pump and seed central wavelengths, the bandwidth, and the relative angles.

V. KERR INSTABILITY CHIRPED PULSE AMPLIFICATION

Once the seed reaches >1% of the pump intensity, the seed and idler saturate, leading to a cascaded four-wave mixing process that generates higher-order beamlets [30,45]. Although these beamlets can be recombined to generate a few-cycle pulse, the difficulty in compensating for the angular dispersion limits this technique for attosecond science

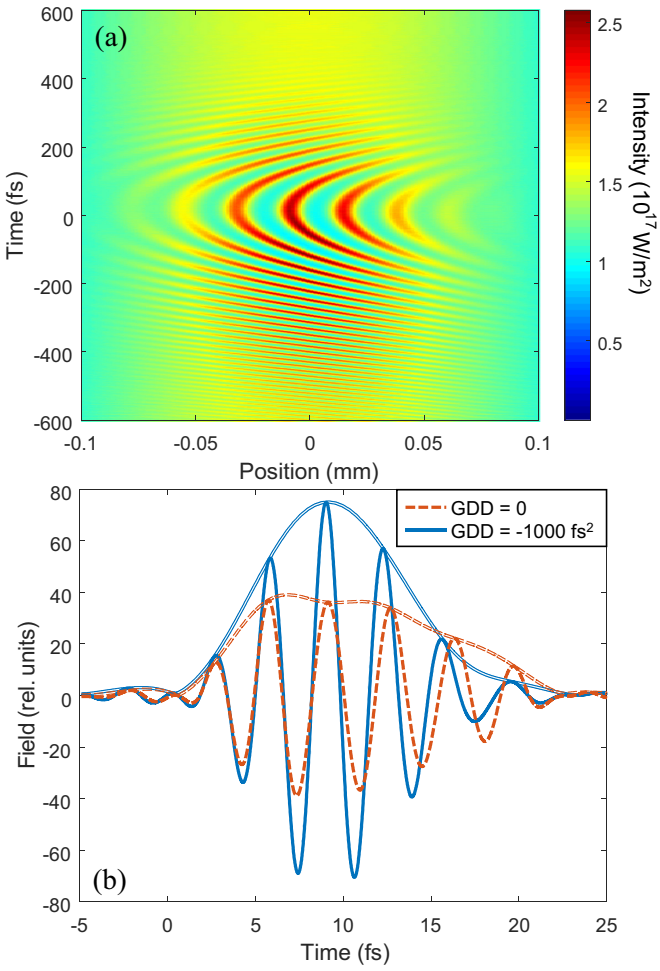

FIG. 8. Applying GDD $= -1000\,\mathrm{fs}^2$ to a 5-fs pulse decreases the peak intensity by $\sim 100\times$, avoiding the saturation effects. (a) Space-time intensity profile of pump and amplified pulse shows a parabolic interference pattern signifying the initial GDD. (b) Amplified field relative to seed for unchirped (dashed orange) and chirped (solid blue) seed fields.

experiments [45–47]. At saturation, we find that the amplified field becomes distorted, leading to beam walk-off and pulse front tilt. Such a result is comparable to noncollinear optical parametric chirped pulse amplifiers [48].

We show the effect of saturation in Fig. 7. When the relative seed to pump intensity, $I_s/I_p = 10^{-6}$ and the seed phase is precompensated, the amplified pulse is below saturation, as shown in Fig. 7(a). In this case, the field demonstrates no spatial distortion to the wavefronts, and the pulse duration is 6.5 fs, close to the input pulse duration of 5 fs. Conversely, with a relative intensity of 6.25×10^{-4}, the saturated amplified pulse is spatially and temporally chirped, as shown in Fig. 7(b).

We find we can avoid saturation by decreasing the peak intensity by chirping the seed. As shown in Fig. 8, we simulate the amplification of a 5-fs seed pulse stretched with GDD $= -1000\,\mathrm{fs}^2$ to decrease its peak intensity by a factor of 110. With chirp, the peak seed intensity relative to the pump is $I_s/I_p = 5.7 \times 10^{-6}$. In this case, the pump, with a central wavelength of 1064 nm, has a top-hat temporal profile of 1500-fs duration. The total intensity of pump and seed is shown in Fig. 8(a) at the exit of the MgO. The parabolic interference demonstrates the seed dispersion, and is below saturation despite the significant intensity modulation. After amplification, we impose $+1000\,\mathrm{fs}^2$ to recompress the pulse, as shown in Fig. 8(b). Without dispersion control, the pulse saturates and the amplified field is $\sim 40\times$ greater than the seed and the pulse duration increases (dashed orange). With the dispersion control, we avoid saturation and the pulse is nearly transform limited (solid blue, pulse duration 6.5 fs) and the peak field strength is $\sim 75\times$ the seed.

VI. CONCLUSION

We find that the GDD of KIA is near zero at the pump wavelength, and follows higher-order dispersion terms over a significant portion of the amplified pulse bandwidth. This imparted phase from the amplification process can be compensated by controlling the seed phase to amplify nearly transform limited few-cycle pulses. The amplified pulse CEP depends on the seed and is nearly independent of the pump. This scheme offers a simple route to generating intense CEP-stable few-cycle pulses. Saturation significantly distorts the amplified field, leading both spatial and temporal chirp. However, chirping the seed can avoid saturation, increasing the amplified pulse peak intensity and enabling Kerr instability chirped-pulse amplification (KICPA).

ACKNOWLEDGMENTS

We acknowledge funding from the Natural Sciences and Engineering Research Council of Canada (Grant No. RGPIN-2019-06877) and the University of Windsor Xcellerate Grant No. 5218522. T.J.H. thanks Thomas Brabec and Claire Duncan for useful conversations.

[1] G. Vampa, T. J. Hammond, M. Nesrallah, A. Y. Naumov, P. B. Corkum, and T. Brabec, Light amplification by seeded Kerr instability, Science **359**, 673 (2018).

[2] S. Ghosh, N. Drouillard, and T. J. Hammond, Supercontinuum amplification by Kerr instability, Phys. Rev. A **109**, 043508 (2024).

[3] S. Ghosh, N. G. Drouillard, and T. J. Hammond, Single-stage few-cycle pulse amplification, Phys. Rev. A **109**, 013511 (2024).

[4] F. Krausz, The birth of attosecond physics and its coming of age, Phys. Scr. **91**, 063011 (2016).

[5] N. Ishii, K. Kaneshima, K. Kitano, T. Kanai, S. Watanabe, and J. Itatani, Carrier-envelope phase-dependent high harmonic generation in the water window using few-cycle infrared pulses, Nat. Commun. **5**, 3331 (2014).

[6] T. J. Hammond, S. Monchocé, C. Zhang, G. Vampa, D. Klug, A. Y. Naumov, D. M. Villeneuve, and P. B. Corkum, Integrating

solids and gases for attosecond pulse generation, Nat. Photonics **11**, 594 (2017).
[7] P. Corkum and F. Krausz, Attosecond science, Nat. Phys. **3**, 381 (2007).
[8] F. Calegari, G. Sansone, S. Stagira, C. Vozzi, and M. Nisoli, Advances in attosecond science, J. Phys. B: At. Mol. Opt. Phys. **49**, 062001 (2016).
[9] M. F. Ciappina, J. A. Pérez-Hernández, A. S. Landsman, W. A. Okell, S. Zherebtsov, B. Förg, J. Schötz, L. Seiffert, T. Fennel, T. Shaaran, T. Zimmermann, A. Chacón, R. Guichard, A. Zaïr, J. W. G. Tisch, J. P. Marangos, T. Witting, A. Braun, S. A. Maier, L. Roso *et al.*, Attosecond physics at the nanoscale, Rep. Prog. Phys. **80**, 054401 (2017).
[10] D. Strickland and G. Mourou, Compression of amplified chirped optical pulses, Opt. Commun. **56**, 219 (1985).
[11] S. Chen, T. Zhou, Q. Du, D. Wang, A. Gilardi, J.-L. Vay, D. Li, J. van Tilborg, C. Schroeder, E. Esarey, R. Wilcox, and C. Geddes, Broadband spectral combining of three pulse-shaped fiber amplifiers with 42 fs compressed pulse duration, Opt. Express **31**, 12717 (2023).
[12] C. Le Blanc, P. Curley, and F. Salin, Gain-narrowing and gain-shifting of ultra-short pulses in Ti: Sapphire amplifiers, Opt. Commun. **131**, 391 (1996).
[13] C. G. Durfee, S. Backus, M. M. Murnane, and H. C. Kapteyn, Design and implementation of a TW-class high-average power laser system, IEEE J. Sel. Top. **4**, 395 (1998).
[14] P. Ji, X. Liu, Z. Huang, X. Lu, K. Liu, Y. Liu, X. Wang, Y. Xu, and Y. Leng, Suppressing the spectral gain-narrowing effect of high-gain Ti: Sapphire amplifiers by a novel polarization-encoded filter, Opt. Commun. **495**, 127086 (2021).
[15] G. Cerullo and S. D. Silvestri, Ultrafast optical parametric amplifiers, Rev. Sci. Instrum. **74**, 1 (2003).
[16] J. Rothhardt, S. Hädrich, J.-C. Delanges, E. Cormier, and J. Limpert, High average power near-infrared few-cycle lasers, Laser Photonics Rev. **11**, 1700043 (2017).
[17] U. Elu, L. Maidment, L. Vamos, F. Tani, D. Novoa, M. H. Frosz, V. Badikov, D. Badikov, V. Petrov, P. S. J. Russel, and J. Biegert, Seven-octave high-brightness and carrier-envelope-phase-stable light source, Nat. Photonics **15**, 277 (2021).
[18] A. Dubietis and A. Matijošius, Table-top optical parametric chirped pulse amplifiers: Past and present, Opto-Electron. Adv. **6**, 220046 (2023).
[19] B. E. Schmidt, N. Thiré, M. Boivin, A. Laramée, F. Poitras, G. Lebrun, T. Ozaki, H. Ibrahim, and F. Légaré, Frequency domain optical parametric amplification, Nat. Commun. **5**, 3643 (2014).
[20] G. Dalla-Barba, G. Jargot, P. Lassonde, S. Tóth, E. Haddad, F. Boschini, J.-C. Delanges, A. Leblanc, H. Ibrahim, E. Cormier, and F. Légaré, Mid-infrared frequency domain optical parametric amplifier, Opt. Express **31**, 14954 (2023).
[21] P. Wang, X. Shen, Z. Zeng, J. Liu, R. Li, and Z. Xu, High-performance seed pulses at 910 nm for 100 pw laser facilities by using single-stage nondegenerate four-wave mixing, Opt. Lett. **44**, 3952 (2019).
[22] M. Nesrallah, G. Vampa, G. Bart, P. B. Corkum, C. R. McDonald, and T. Brabec, Theory of Kerr instability amplification, Optica **5**, 271 (2018).
[23] N. Bloembergen, Conservation laws in nonlinear optics, J. Opt. Soc. Am. **70**, 1429 (1980).
[24] H. Valtna, G. Tamoauskas, A. Dubietis, and A. Piskarskas, High-energy broadband four-wave optical parametric amplification in bulk fused silica, Opt. Lett. **33**, 971 (2008).
[25] G. Agrawal, *Nonlinear Fiber Optics*, 3rd ed. (Academic, New York, 2001).
[26] C. Manzoni and G. Cerullo, Design criteria for ultrafast optical parametric amplifiers, J. Opt. **18**, 103501 (2016).
[27] M. Galletti, G. Archipovaite, P. Oliveira, M. Galimberti, I. Musgrave, and C. Hernandez-Gomez, Broadband, picosecond two-stage optical parametrical chirped pulse amplification system at 100 Hz, Phys. Rev. Accel. Beams **22**, 051301 (2019).
[28] A. V. Husakou and J. Herrmann, Supercontinuum generation of higher-order solitons by fission in photonic crystal fibers, Phys. Rev. Lett. **87**, 203901 (2001).
[29] L. Bergé, S. Skupin, R. Nuter, J. Kasparian, and J.-P. Wolf, Ultrashort filaments of light in weakly ionized, optically transparent media, Rep. Prog. Phys. **70**, 1633 (2007).
[30] C. J. Arachchige, J. A. Stephen, and T. J. Hammond, Amplification of femtosecond pulses based on $\chi^{(3)}$ nonlinear susceptibility in MgO, Opt. Lett. **46**, 5521 (2021).
[31] A. Jullien, L. Canova, O. Albert, D. Boschetto, L. Antonucci, Y.-H. Cha, J. P. Rousseau, P. Chaudet, G. Chériaux, J. Etchepare, S. Kourtev, N. Minkovski, and S. M. Saltiel, Spectral broadening and pulse duration reduction during cross-polarized wave generation: Influence of the quadratic spectral phase, Appl. Phys. B **87**, 595 (2007).
[32] A. Jullien, J.-P. Rousseau, B. Mercier, L. Antonucci, O. Albert, G. Chériaux, S. Kourtev, N. Minkovski, and S. M. Saltiel, Highly efficient nonlinear filter for femtosecond pulse contrast enhancement and pulse shortening, Opt. Lett. **33**, 2353 (2008).
[33] S. Xu, T. Jia, H. Sun, C. Li, X. Li, D. Feng, J. Qiu, and Z. Xu, Mechanisms of femtosecond laser-induced breakdown and damage in MgO, Opt. Commun. **259**, 274 (2006).
[34] J. Ma, K. Xiong, P. Yuan, X. Tu, J. Wang, G. Xie, Y. Zheng, and L. Qian, Demonstration of 85 noise content in quasi-parametric chirped-pulse amplification, Light sci. appl. **11**, 1 (2022).
[35] P. Tournois, Acousto-optic programmable dispersive filter for adaptive compensation of group delay time dispersion in laser systems, Opt. Commun. **140**, 245 (1997).
[36] A. M. Weiner, Ultrafast optical pulse shaping: A tutorial review, Opt. Commun. **284**, 3669 (2011).
[37] V. Loriot, G. Gitzinger, and N. Forget, Self-referenced characterization of femtosecond laser pulses by chirp scan, Opt. Express **21**, 24879 (2013).
[38] K.-H. Hong, J. Lee, B. Hou, J. A. Nees, E. Power, and G. A. Mourou, Carrier-envelope phase stabilization of high-contrast femtosecond laser pulses with a relativistic intensity, Appl. Phys. Lett. **89**, 031113 (2006).
[39] F. Frank, C. Arrell, T. Witting, W. A. Okell, J. McKenna, J. S. Robinson, C. A. Haworth, D. A. H. Teng, I. A. Walmsle, J. P. Marangos, J. W. G. Tisch, P. Martinez, and P. Noé, Technology for attosecond science, Rev. Sci. Instrum. **83**, 071101 (2012).
[40] F. Lücking, V. Crozatier, N. Forget, A. Assion, and F. Krausz, Approaching the limits of carrier-envelope phase stability in a millijoule-class amplifier, Opt. Lett. **39**, 3884 (2014).
[41] T. Balčiūnas, O. Mücke, P. Mišeikis, G. Andriukaitis, A. Pugžlys, L. Giniūnas, R. Danielius, R. Holzwarth, and A. Baltuška, Carrier envelope phase stabilization

of a Yb: KGW laser amplifier, Opt. Lett. **36**, 3242 (2011).

[42] T. Balčiūnas, T. Flöry, A. Baltuška, T. Stanislauskas, R. Antipenkov, A. Varanavičius, and G. Steinmeyer, Direct carrier-envelope phase control of an amplified laser system, Opt. Lett. **39**, 1669 (2014).

[43] E. Cunningham, Y. Wu, and Z. Chang, Carrier-envelope phase control of a 10 Hz, 25 TW laser for high-flux xuv continuum generation, Appl. Phys. Lett. **107**, 201108 (2015).

[44] D. J. Jones, S. T. Cundiff, T. M. Fortier, J. L. Hall, and J. Ye, Carrier envelope phase stabilization of single and multiple femtosecond lasers, in *Few-Cycle Laser Pulse Generation and its Applications*, edited by F. X. Kärtner (Springer, Berlin, 2004), Vol. 95, pp. 317–343.

[45] R. Weigand and H. M. Crespo, Fundamentals of highly non-degenerate cascaded four-wave mixing, Appl. Sci **5**, 485 (2015).

[46] T. Kobayashi, J. Liu, and K. Okamura, Applications of parametric processes to high-quality multicolour ultrashort pulses, pulse cleaning and cep stable sub-3 fs pulse, J. Phys. B: At. Mol. Opt. Phys. **45**, 074005 (2012).

[47] J. He, J. Liu, and T. Kobayashi, Tunable multicolored femtosecond pulse generation using cascaded four-wave mixing in bulk materials, Appl. Sci. **4**, 444 (2014).

[48] A. Giree, M. Mero, G. Arisholm, M. J. J. Vrakking, and F. J. Furch, Numerical study of spatiotemporal distortions in noncollinear optical parametric chirpedpulse amplifiers, Opt. Express **25**, 3104 (2017).